Supporting Information for:

The Influence of Perovskite Crystal Structure on Its Stability

*Hualin Bi[a], Mengke Wang[a], Lei Liu[a], Jiahe Yan[a], Rongfei Zeng[b], Zhang Xu[c], Jun Wang[a]**

aDepartment of Chemistry, College of Sciences, Northeastern University, Shenyang 110819, P. R. China

bCollege of Software Northeastern University, Shenyang 110819, P. R. China

cState Key Laboratory of Fine Chemicals, Dalian University of Technology, Dalian 116023, P. R. China.

*E-mail: wangjun12@mail.neu.edu.cn

Table of Contents

COMPUTATIONAL DETAILS S3

1.1 MD Simulation……...……S3

1.2 Adsorption Model crystal structure……...…….S6

1.3 DNN design and training…….……...……S8

1.4 CCMMOE design and training……...……..S11

1.5 CCMMOE exploration……S17

1.6 SHAP calculation……..S22

1.7 SHAP results discussed……..……..S22

EXPERIMENTAL SECTION……..……S27

REFERENCE……S36

Computational Details

1.1MD Simulation

Molecular dynamics simulations were performed using the Absorption and Forcite of Materials Studio (2017) designed by Accelrys, Inc., San Diego, CA. Ensemble simulations were conducted under constant particle number, constant pressure, and constant temperature (NPT) conditions for the constructed and minimized adsorption system at various temperature and pressure settings. To determine the interaction strengths of gas molecules on the (110) crystal plane of hybrid organic-inorganic perovskite, three models were established: a three-dimensional model consisting of a gas molecule on the hybrid organic-inorganic perovskite surface, the hybrid organic-inorganic perovskite surface only, and the gas molecules only. The COMPASS force field was utilized to calculate the interaction potential energy. NPT simulations for the three-dimensional models were conducted for 100 ps with a time step of 1 fs. Prior to MD simulations, all systems underwent energy minimization for structural optimization. The adsorption energy of different molecules on the hybrid organic-inorganic perovskite surface can be calculated as follows: $E_{adsorption} = E_{total} - (E_{substrate} + E_{gas})$, where $E_{adsorption}$ represents the adsorption energy, E_{total} is the total system energy, $E_{substrate}$ is the substrate energy, and Egas is the total energy of the adsorbate gas molecules. Using a similar approach, the adsorption energy of different adsorbate molecules (including 2 H_2O molecules, 5 H_2O molecules, 7 H_2O molecules, 10 H_2O molecules, 5 CO molecules, 5 SO_2 molecules, 5 NH_3 molecules, 5 CH_4 molecules, 5

C_3H_6O molecules, and $5C_4H_{10}O$ molecules) on the surface of 1049 hybrid organic-inorganic perovskite structures was calculated.

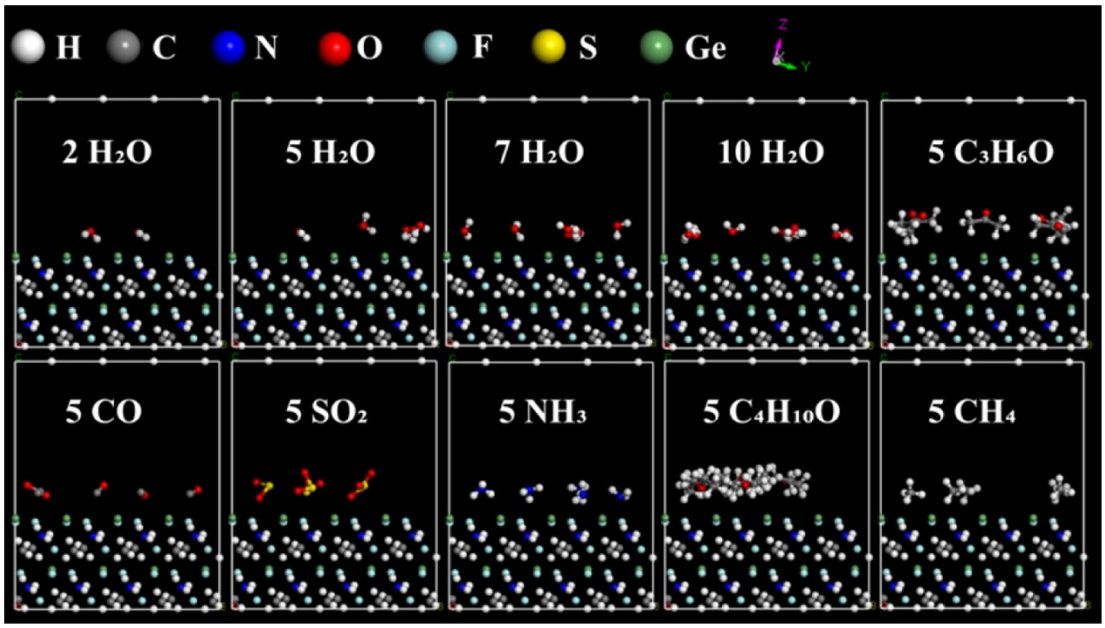

Figure S1. Molecular Dynamics (MD) simulation results of 10 gas molecules on the $MAGeF_3$ (110) plane. The related MD Simulations were performed using Discover and Amorphous Cell modules of Materials Studio.

1.2 Adsorption Model crystal structure

The adsorption model voxelization process involves converting the original CIF file into a tensor of shape (number of element types, voxel count X, voxel count Y, voxel count Z) and transforming the coordinates of each atom into (voxel index X_i, voxel index Y_i, voxel index Z_i). The conversion steps are as follows: First, we obtain the maximum and minimum atomic coordinates in each direction (XYZ) within the entire adsorption model: X_{max}, X_{min}, Y_{max}, Y_{min}, Z_{max}, Z_{min}. Then, we create a space with dimensions ($X_{max} - X_{min}$), ($Y_{max} - Y_{min}$), and ($Z_{max} - Z_{min}$), and partition this space into small voxels, determining the number of voxels (1) in each direction X, Y, and Z, with ΔX, ΔY, and ΔZ being the chosen voxel sizes.

$$\begin{aligned} &\text{Number of Voxels X} = (X_{max} - X_{min}) / \Delta X \\ &\text{Number of Voxels Y} = (Y_{max} - Y_{min}) / \Delta Y \\ &\text{Number of Voxels Z} = (Z_{max} - Z_{min}) / \Delta Z \end{aligned} \qquad (1)$$

Finally, we map the atomic coordinates to the voxel grid nodes. For each atom's three-dimensional coordinates (X_i, Y_i, Z_i), we use the following formula to map them to the nearest voxel grid node, resulting in each atom's coordinates being transformed into (Voxel Index X_i, Voxel Index Y_i, Voxel Index Z_i) (2).

$$\begin{aligned} &\text{Voxel Index } X_i = (X_i - X_{min}) / \Delta X \\ &\text{Voxel Index } Y_i = (Y_i - Y_{min}) / \Delta Y \\ &\text{Voxel Index } Z_i = (Z_i - Z_{min}) / \Delta Z \end{aligned} \qquad (2)$$

This step is crucial as it ensures that the processed adsorption model can be handled by three-dimensional convolutional layers.

After voxelization, crystals may have non-uniform sizes, making them unsuitable for direct input into the model. To address this, we've utilized the scipy.ndimage.zoom function to uniformly scale them to a size of 32x32x32.

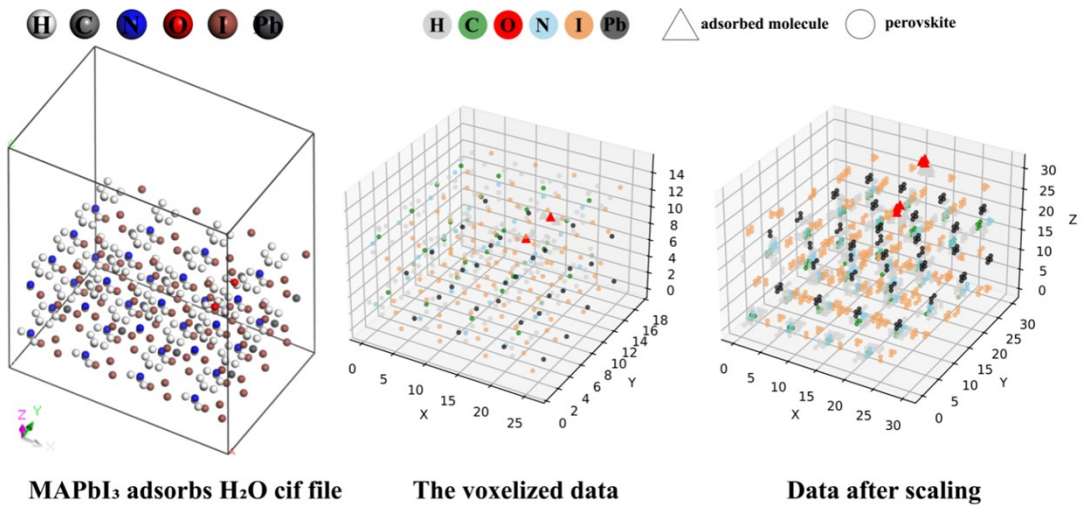

Figure S2. Adsorption Model crystal structure conversion process.

1.2DNN train

All model constructions in this paper were implemented using the PyTorch framework.

The input for the DNN consists of the three-dimensional coordinates of three halogen atoms, the three-dimensional coordinates of one metal atom, the type of halogen atoms, the type of metal atom, and the type of organic molecule (both atom and molecule types are one-hot encoded). The output of the DNN is the corresponding adsorption energy.

The DNN training utilizes the Adam optimizer, L1 loss function, with a learning rate set to 0.001, and trains for 100 epochs. After training, the DNN model achieved Mean Absolute Error (MAE) values of 2.8271 and 4.2033 kcal/mol on the training and test sets, respectively.

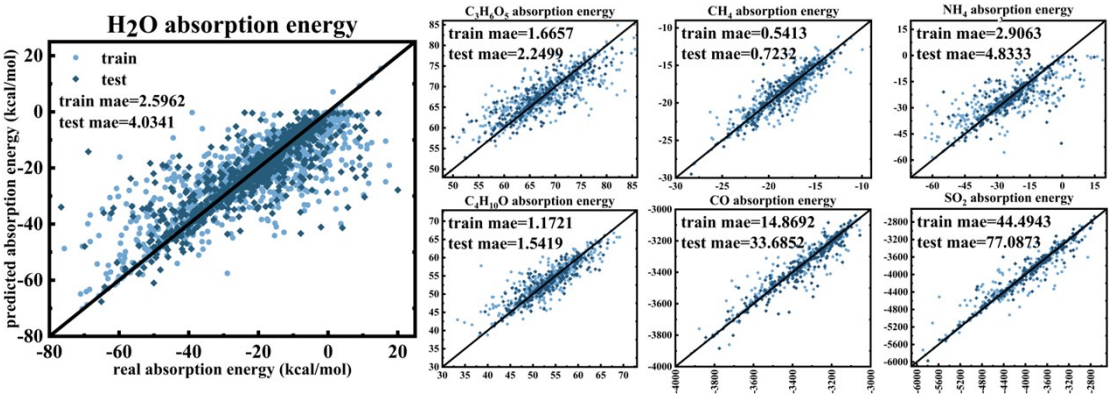

Figure S3.MAE of the DNN model in training and test sets of adsorption energy data.

Table S1. The DNN architecture was adopted in this study

layer	type	Size of output	activation
In	Input	44	
L1	Linear	48	LeakyReLU
L2	Linear	48	LeakyReLU
L3	Linear	24	LeakyReLU
L4	Linear	12	LeakyReLU
L5	Linear	6	LeakyReLU
Out	Linear	1	LeakyReLU

1.4CCMMOE design and training

The CCMMOE model is constructed based on the MMOE model [1], incorporating redesigned expert groups and gating networks. In the CCMMOE model, each expert is primarily composed of 3D convolutional layers, after each of which coordinate attention is applied [2]. The coordinate attention considers its positional relationships based on channel attention and combines primary channel attention with spatial attention. It's worth noting that some modifications were made on the original coordinate attention to make it capable of handling volumetric data. A new dimension Z was added, which changes the original 2D convolution layers to 3D ones. After the 3D convolutional layers, the data were flattened and fully connected layers were added. The output of each expert is one-dimensional data with a shape of 64. In this work, 10 experts were set up to constitute the expert group of the CCMMOE model.

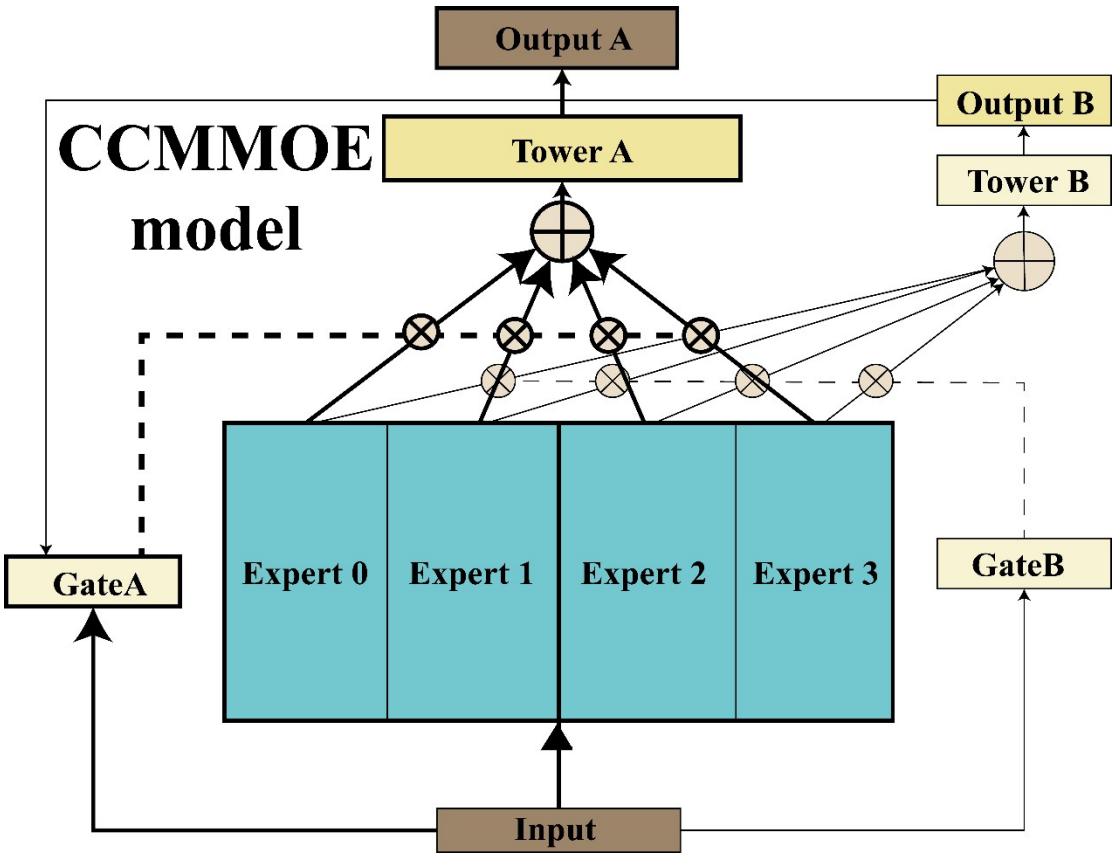

Figure S4. CCMMOE model frame.

Table S2. expert net

layer	type	Size of output	Kernel size	stride	activation
In	Input	13*32*32*32			
C1	Conv3d	256*16*16*16	2*2*2	2	LeakyReLU
CA1	Coordinate Attention	256*16*16*16			
B1	BatchNorm3d	256*16*16*16			
A1	AvgPool3d	256*8*8*8	2*2*2	2	
C2	Conv3d	256*4*4*4	2*2*2	2	LeakyReLU
CA2	Coordinate Attention	256*4*4*4			
B2	BatchNorm3d	256*4*4*4			
A2	AvgPool3d	256*2*2*2	2*2*2	2	
F1	Flatten	256*8			
L1	Linear	256			LeakyReLU
Out	Linear	64			LeakyReLU

Two gating networks, i.e., gateA and gateB, were set up in this study. The structure of each gating network begins with a 3D convolutional layer for dimension reduction, followed by a flattening step and a fully connected layer. The gateA is divided into two parts: gateA-1 and gateA-2. The gateA-1 and gateB have the same structure with an output dimension equal to the number of experts. On the other hand, gateA-2 takes as input the concatenation of the inputs to gateA-1 and gateB, resulting in an input dimension that is twice the number of experts. After passing through a fully connected layer and an activation function, the output dimension of gateA-2 also matches the number of experts.

Table S3. gateA-1

layer	type	Size of output	Kernel size	stride	activation
In	Input	13*32*32*32			
C1	Conv3d	4*16*16*16	2*2*2	2	LeakyReLU
B1	BatchNorm3d	4*16*16*16			
A1	AvgPool3d	4*8*8*8	2*2*2	2	
F1	Flatten	4*512			
Out	Linear	10			LeakyReLU

Table S4. gateA-2

layer	type	Size of output	Kernel size	stride	activation
In	Input	20			
L1	Linear	16			LeakyReLU
Out	Linear	10			Softmax

Table S5. gateB

layer	type	Size of output	Kernel size	stride	activation
In	Input	13*32*32*32			
C1	Conv3d	4*16*16*16	2*2*2	2	LeakyReLU
B1	BatchNorm3d	4*16*16*16			
A1	AvgPool3d	4*8*8*8	2*2*2	2	
F1	Flatten	4*512			
Out	Linear	10			Softmax

Table S6. TowerA

layer	type	Size of output	Kernel size	stride	activation
In	Input	640			
L1	Linear	128			LeakyReLU
Out	Linear	1			LeakyReLU

Table S7. TowerB

layer	type	Size of output	Kernel size	stride	activation
In	Input	640			
L1	Linear	128			LeakyReLU
Out	Linear	10			LeakyReLU

The input for CCMMOE is the voxelized adsorption model (with a shape of 13*32*32*32), and the output is the corresponding adsorption energy. For the training of outputA, Adam optimizer and L1 loss function were used, with a learning rate set to 0.0001. For outputB, Adam optimizer and CrossEntropy loss function were employed. After training, the MAE values for outputA on the test and training sets were determined to be 4.3612 and 6.3082 kcal/mol, respectively. Regarding outputB, the accuracy on the test and training sets were 94.8913% and 98.9068%, respectively.

1.5CCMMOE exploration

1.5.1 Influence of different voxel sizes on training results

We tested the influence of different voxel sizes on the training effectiveness of the CCMMOE model. The training parameters were set as follows: learning rate of 0.00001 and 20 epochs. Voxel sizes were set to 0.5 Å, 0.75 Å, 1 Å, 1.25 Å, and 1.5 Å. Through experimentation, we found that setting the voxel size to 1 Å yielded the best overall results. When the voxel size was greater than 1 Å, although theoretically preserving the least amount of information and achieving better accuracy, the decrease in Mean Absolute Error (MAE) during training slowed down significantly, leading to substantial storage and computational burdens. Additionally, to maintain consistent model parameters, we uniformly scaled the data to a size of 32 * 32 * 32. Therefore, adopting smaller voxel sizes had little significance. When the voxel size was less than 1 Å, the MAE of the model decreased rapidly during training; however, compared to the 1 Å voxel size, the model ultimately achieved inferior results. Thus,

given acceptable computational and storage capabilities, we ultimately chose 1 Å as the voxel size.

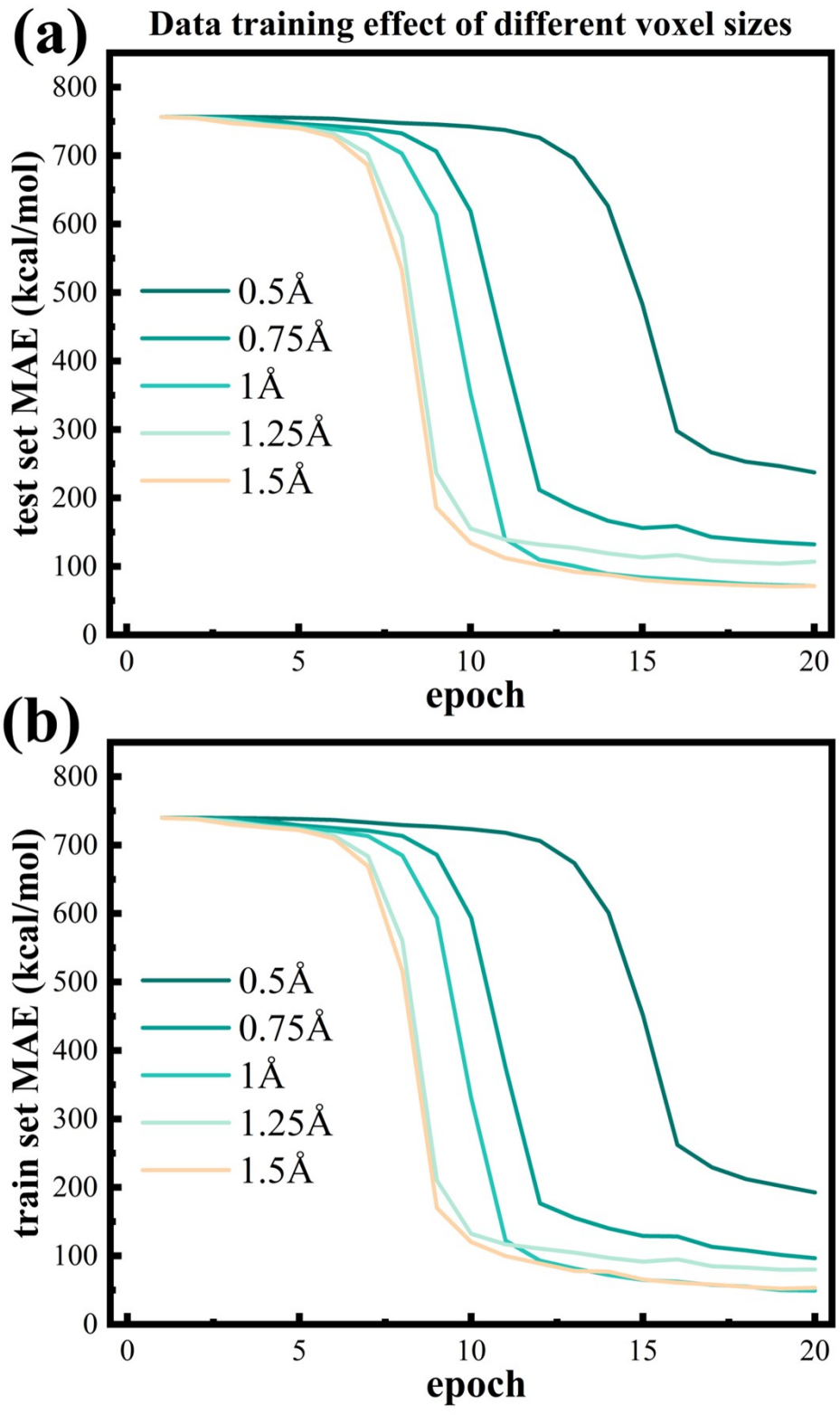

Figure S5. Influence of different voxel sizes on training results.

1.5.2 Comparison of expert network and CCMMOE training.

We also compared the training effectiveness between a single expert network and the CCMMOE model. For the single expert network, we appended two additional linear layers at the end to allow it to directly output without passing through OutputA. The learning rate was set to 0.00001, and training was conducted for 20 epochs. Compared to the ten expert networks in CCMMOE, the single expert network is lighter and easier to train; however, its final training performance is inferior to that of CCMMOE.

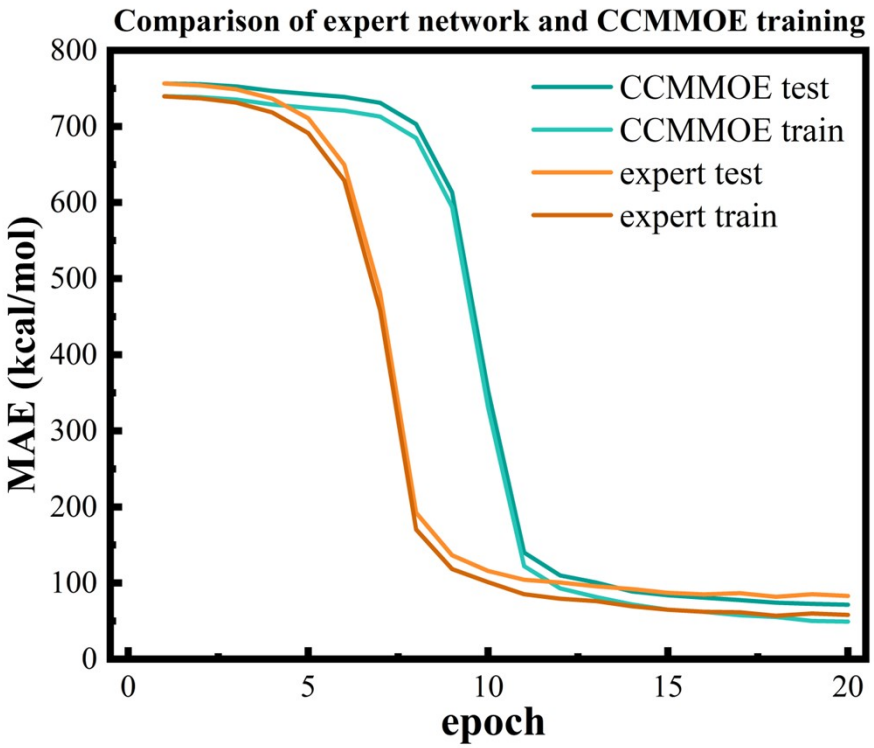

Figure S6. Comparison of expert network and CCMMOE training.

1.6SHAP calculation

The SHAP value calculation utilized the GradientShap function from the captum library [3], and the parameters for SHAP value computation were consistent for both the DNN and CCMMOE models. The baseline was set to a zero matrix with the same shape as the input, and stdevs were set to 0.1. During computation, SHAP values were only calculated for the adsorption model concerning adsorption of water molecules.

1.7SHAP results discussed

1.71 SHAP value analysis of organic molecules

In addition to halides, organic cations are also crucial components of organo-inorganic hybrid perovskites, significantly impacting their adsorption energy. We conducted a SHAP value analysis on a DNN model and found that among the organic cations, $OHNH_3$ has the most significant influence on increasing the adsorption energy, followed by commonly used methylamine and ethylamine.

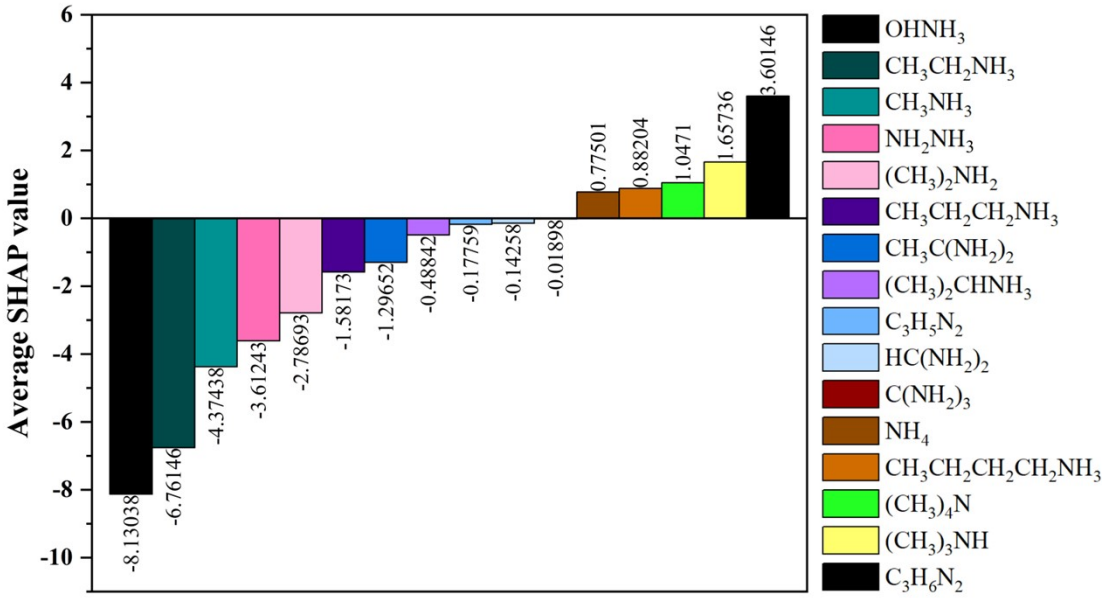

Figure S7. Cationic SHAP value.

1.72CCMMOE model SHAP value display

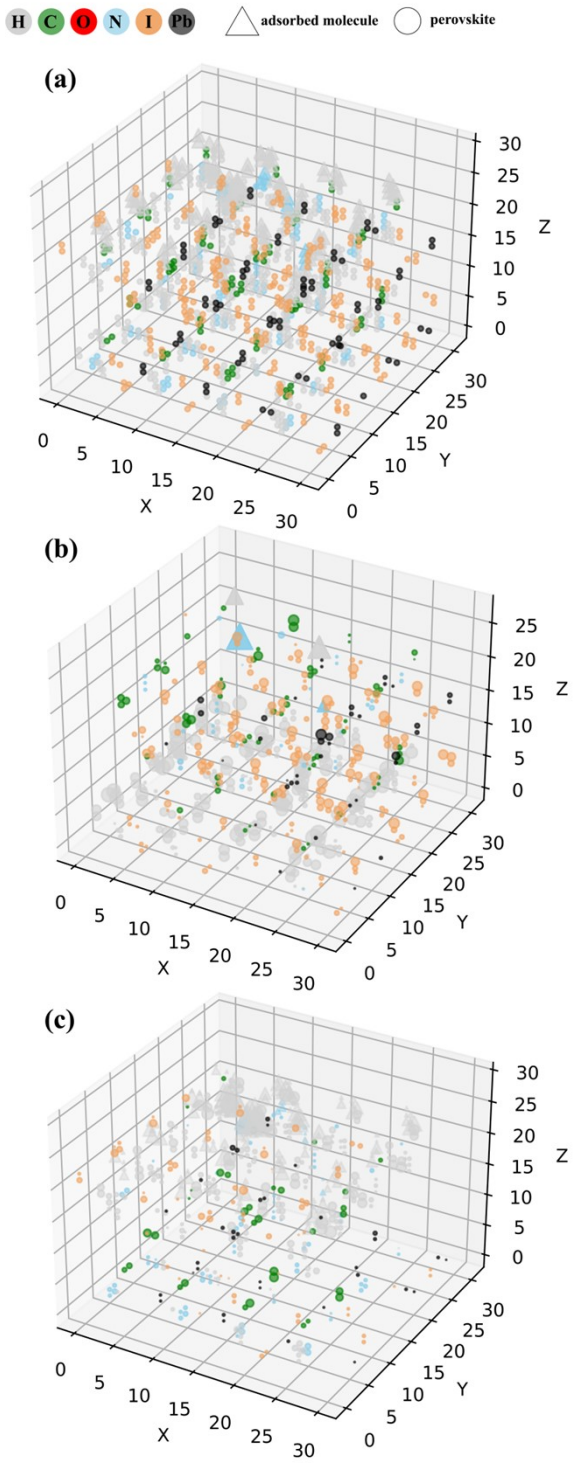

Figure S8. $MAPbI_3$ adsorption NH_3 SHAP value distribution. The triangle represents the adsorbed molecule, and the circle represents the perovskite substrate. The size of the scatter plot represents the magnitude of the absolute SHAP values, calculated by the CCMMOE model.

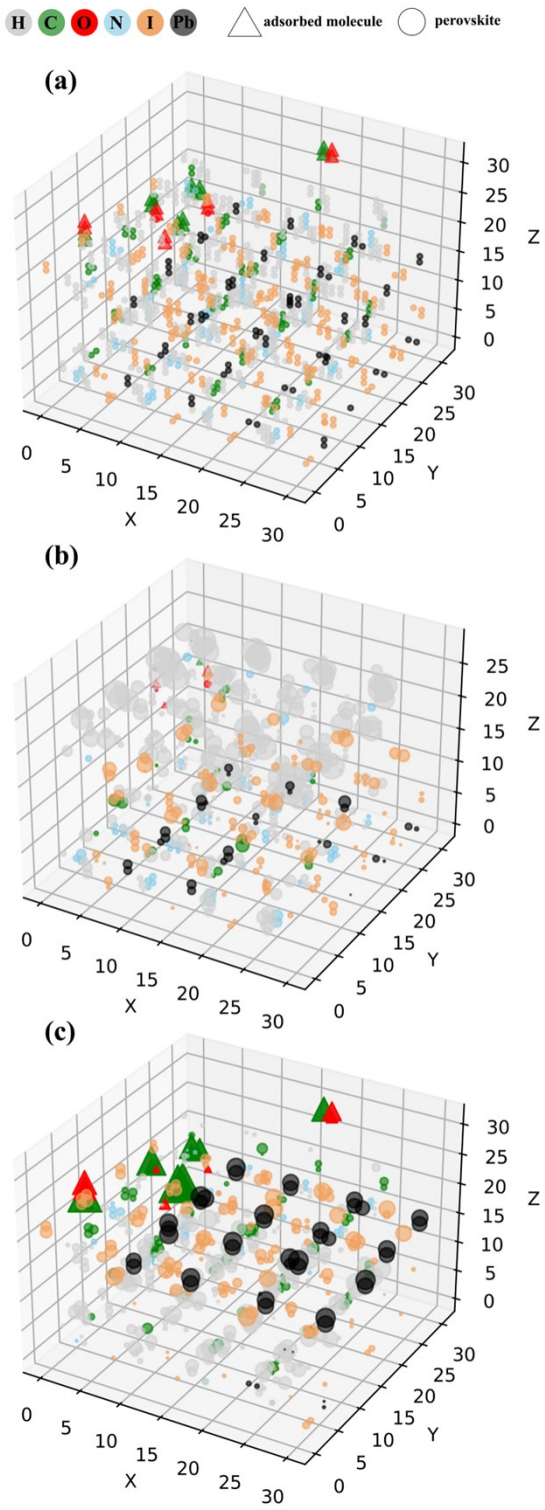

Figure S9. $MAPbI_3$ adsorption CO SHAP value distribution. The triangle represents the adsorbed molecule, and the circle represents the perovskite substrate. The size of the scatter plot represents the magnitude of the absolute SHAP values, calculated by the CCMMOE model.

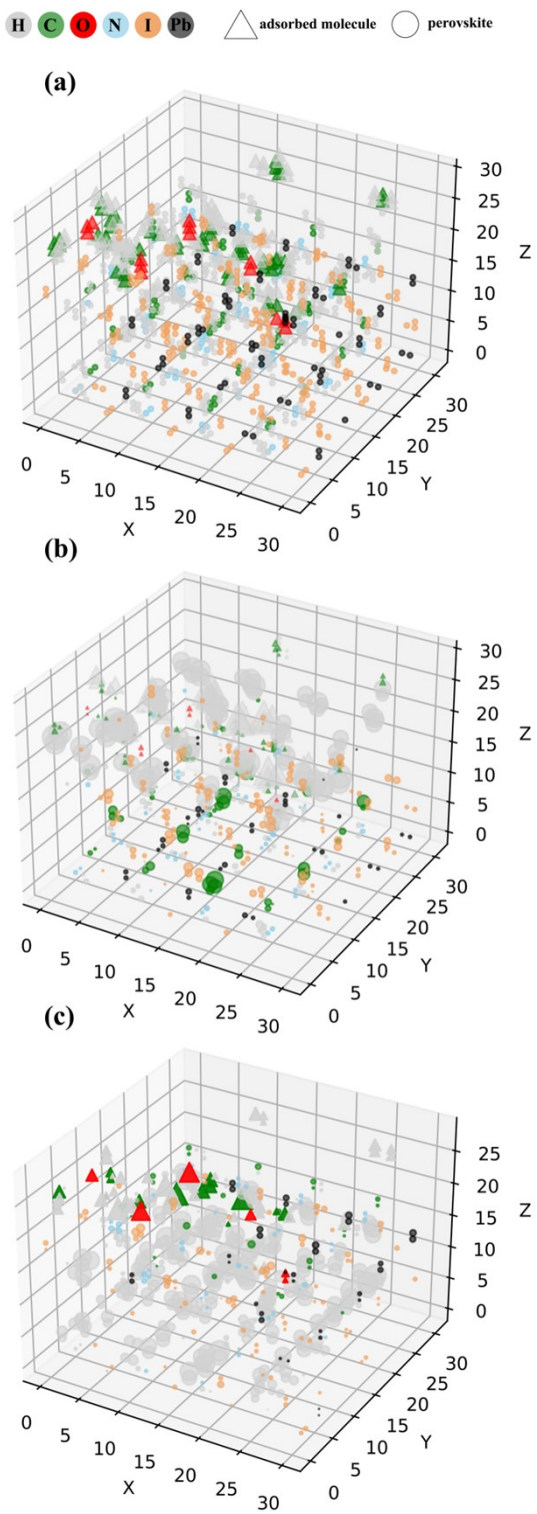

Figure S10. $MAPbI_3$ adsorption $C_4H_{10}O$ SHAP value distribution. The triangle represents the adsorbed molecule, and the circle represents the perovskite substrate. The size of the scatter plot represents the magnitude of the absolute SHAP values, calculated by the CCMMOE model.

Experimental Section

The reliability of SHAP analysis was verified experimentally with nine $MAPbX_3$-type perovskites prepared in this work, namely $MAPbCl_3$, $MAPbCl_{2.25}Br_{0.75}$, $MAPbCl_{1.5}Br_{1.5}$, $MAPbCl_{0.75}Br_{2.25}$, $MAPbBr_3$, $MAPbBr_{2.25}I_{0.25}$, $MAPbBr_{1.5}I_{1.5}$, $MAPbBr_{0.75}I_{2.25}$, and $MAPbI_3$. To give an example, the $MAPbI_3$ perovskite was prepared by spin coating a solution containing PbI_2, MAI and DMSO onto an electrode, followed by drying at 60 °C for 20 min to evaporate the solvent (Fig. 4a). The structures of the perovskites were characterized and confirmed by X-ray diffraction (XRD) (Fig. 4b) and UV-vis absorption spectroscopy (Fig. 4c). In a typical process of the experiment, the perovskite samples were placed in a dark and sealed container under a certain voltage, and the change in the current after adding water was measured. Due to the significant differences in the electrical properties of the varied perovskites, different voltage values were applied to the samples. Once a stable current was achieved for each perovskite, 5 ml of water was injected into the sealed container, where the liquid water was evaporated into the gaseous phase with the equipped ceramic heating unit. Subsequently, another 5 ml of water was introduced 5 min after the first water addition. The tests were conducted after each addition of water, and the experiments were repeated 3 times. Based on the obtained current curves for the nine perovskites at different humidity levels, the average values of the response rates were calculated according to the formula below:

$$I_{\text{response rate}} = (I_{\text{current value}} - I_{\text{initial value}})/ I_{\text{initial value}} \qquad (1)$$

By mapping the average response rate, it was found that the response rate after the second water addition is higher than that of the first time, and it changes with the content of Cl, Br and I in the perovskites. More importantly, the perovskite containing Cl showed the lowest response rate, indicating its highest stability against water and the smallest adsorption energy for water molecules. On the contrary, the I-containing perovskite exhibited the largest response rate value and lowest stability to water. However, the stability of halogen-doped perovskites is always higher than that of the pure perovskite [4][5][6]. We also measured the PL of $MAPbI_3$, $MAPbBr_3$, and $MAPbCl_3$ perovskites on the 0th, 2nd, 5th, and 10th days after preparation. The results revealed that $MAPbI_3$ exhibited the least decrease in luminescence intensity, while $MAPbCl_3$ showed the most significant decrease. These experimental results are consistent with the data from SHAP analysis.

Materials: All chemical reagents were purchased from commercial vendors and are as follows: Lead (II) iodide (PbI_2, 99%, Sigma-Aldrich), Lead (II) bromide ($PbBr_2$, 99%, Sigma-Aldrich), Lead (II) chloride ($PbCl_2$, 99%, Sigma-Aldrich), Methylamine iodide (CH_6IN, 98%, Macklin), Methylamine bromide (CH_6BrN, 99.5%, Macklin), Methylamine hydrochloride (CH_6ClN, 98%, Macklin), Dimethyl sulfoxide (DMSO, 99.8%, with molecular sieves, water ≤50 ppm, Macklin). All reagents were used as received without further purification, and all aqueous solutions were prepared with deionized water (>18 MΩ).

The synthesis of $MAPbI_3$ is as follows: First, 0.461 grams (1 mmol) of lead (II)

iodide powder were dissolved in 1 milliliter of dimethyl sulfoxide (DMSO) along with 0.159 grams (1 mmol) of methylamine iodide powder. The solution was heated and stirred until it became clear, and then it was filtered through a nylon 66 filter plug for subsequent use.

The synthesis of $MAPbI_{2.25}Br_{0.75}$, $MAPbI_{0.75}Br_{2.25}$, $MAPbBr_3$, $MAPbBr_{2.25}Cl_{0.75}$, $MAPbBr_{1.5}Cl_{1.5}$, $MAPbBr_{0.75}Cl_{2.25}$, $MAPbCl_3$ preparation process is similar to the above.

Fabrication of Film and Device: First, the interdigitated electrode (with a gap width of 100 μm on a PET substrate) was rinsed with ethanol and thoroughly dried. Next, 5 μL of the prepared $MAPbX_3$ perovskite solution was dropped onto the interdigitated electrode, and the electrode was further dried at 60 °C on a hotplate for 10 minutes.

Testing environment: During the test, with ambient humidity lower than 30% and the temperature around 10 degrees Celsius, the perovskite film was shielded from light.

Characterization and Measurements: XRD patterns were characterized using a powder X-ray diffractometer (Empyrean, PANalytical B.V.) with Cu Kα1 radiation (λ = 1.5406 Å). Absorption spectra were acquired using a UV-vis spectrophotometer (Lambda 650S, PerkinElmer). The surface morphology was examined using a field-emission scanning electron microscope (SU8010, HITACHI) coupled with EDS. All

electrical measurements were carried out using a probe station coupled to a Keithley2450.

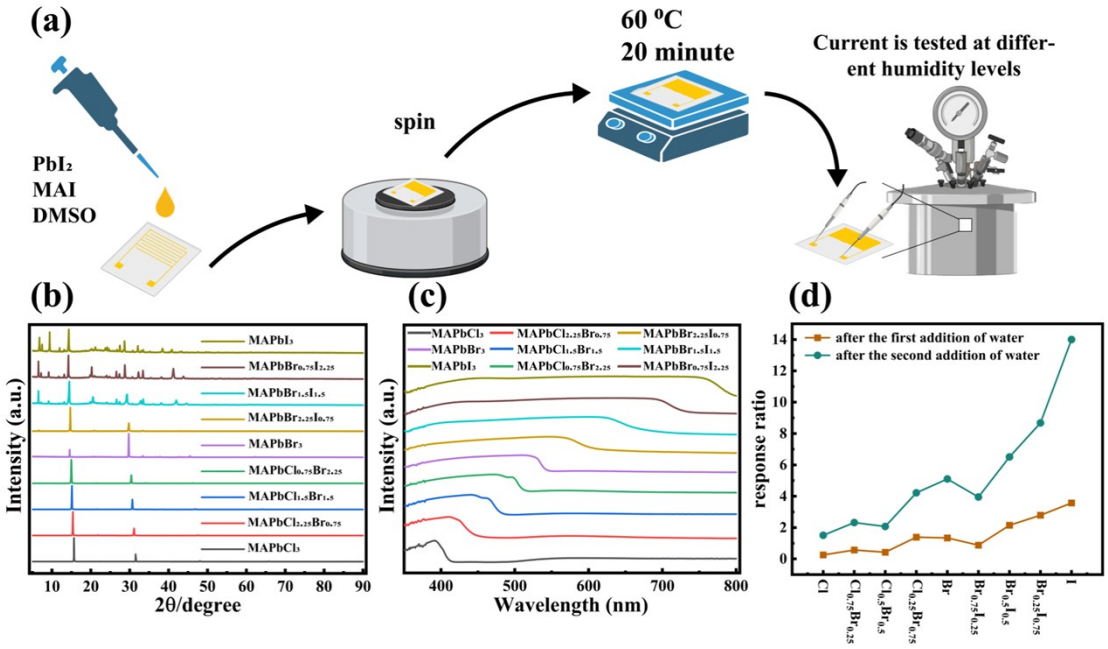

FigureS11. Schematic diagram of the $MAPbI_3$ preparation process (a). XRD patterns (b), UV-vis spectra (c) and response rates (d) of the nine $MAPbX_3$ type perovskites.

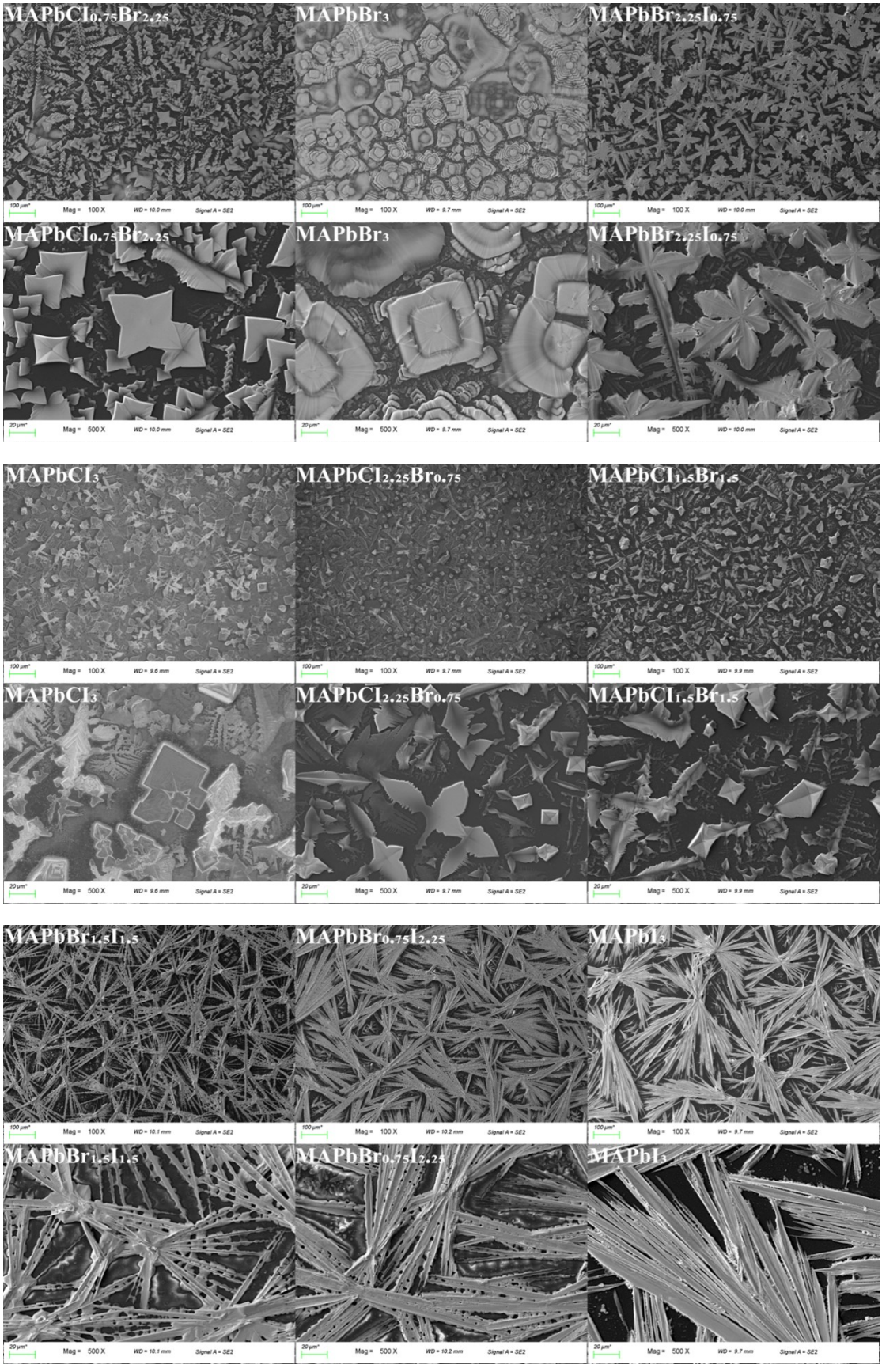

Figure S12. HRTEM micrographs of 9 kinds of $MAPbX_3$ type perovskites.

Figure S13. 9 kinds of $MAPbX_3$ type perovskites. Perovskite solution is spun onto a glass plate, and the solvent is steamed to take pictures.

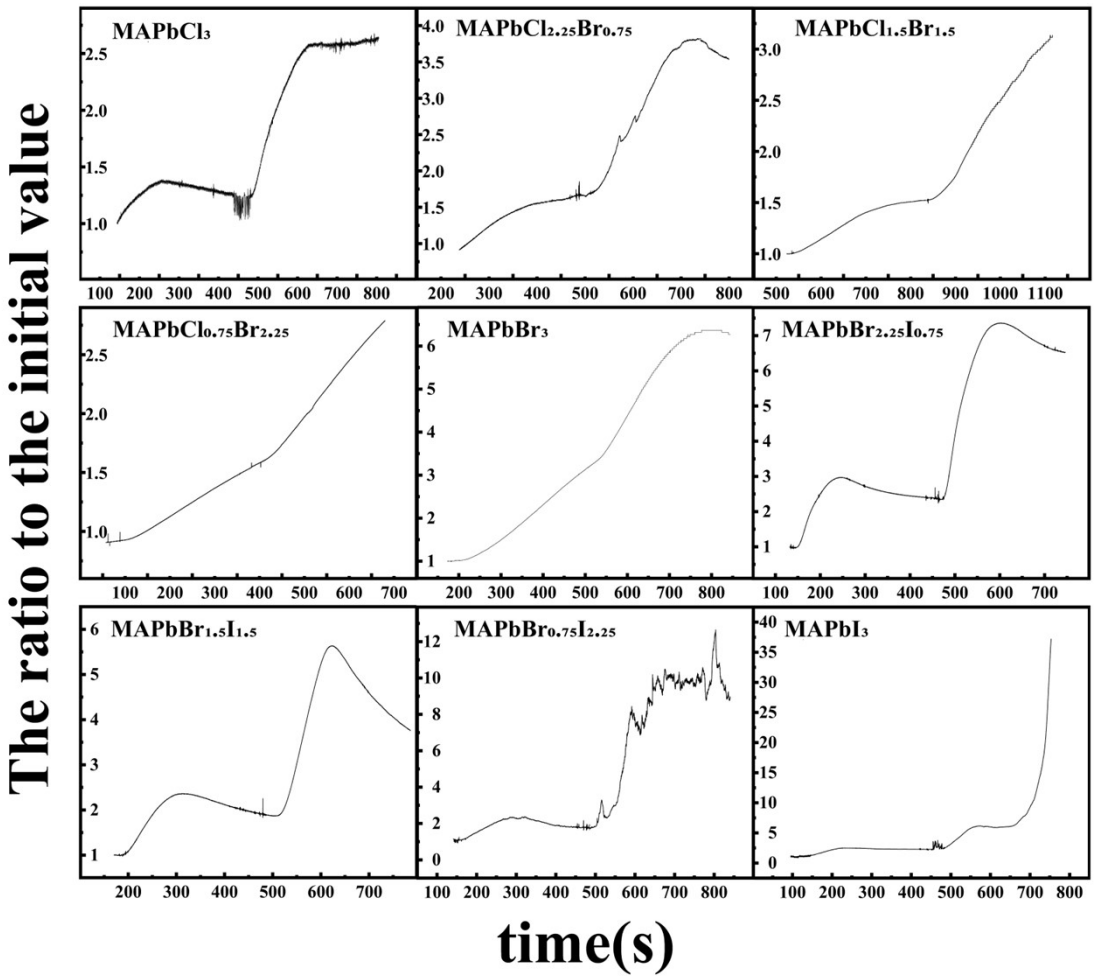

Figure S14. Electrical experimental curves of 9 $MAPbX_3$ type perovskites. Put the prepared perovskite device into a closed container, pass the appropriate voltage, record the response rate of the current over time, each time adding water interval of 5 minutes, each time adding water of 5 microliters, the added water will be quickly evaporated into a gas by the ceramic heating plate in the container.

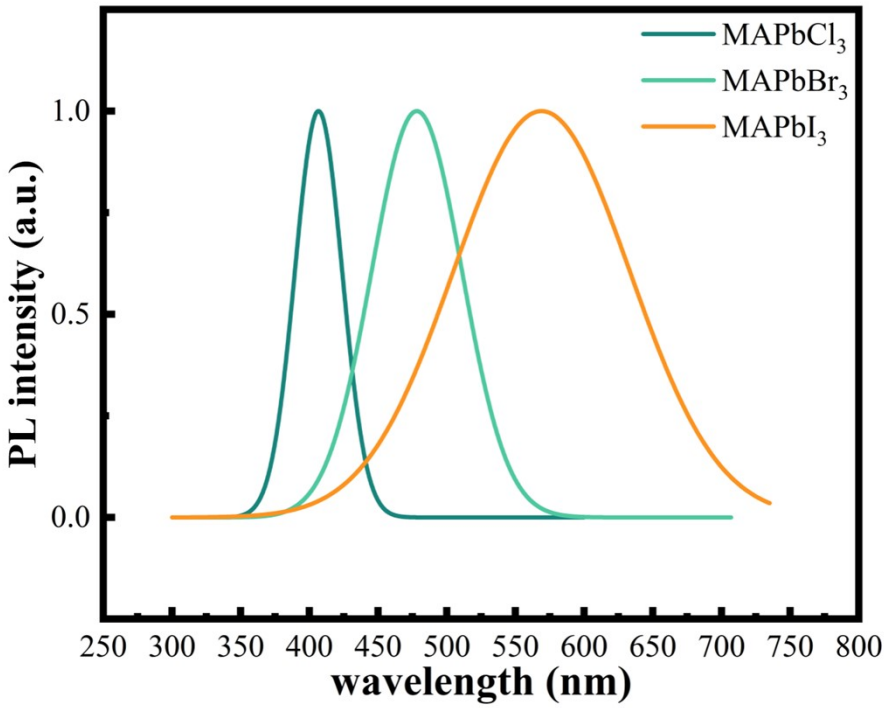

Figure S15. The PL spectra of freshly prepared $MAPbI_3$, $MAPbBr_3$, and $MAPbCl_3$.

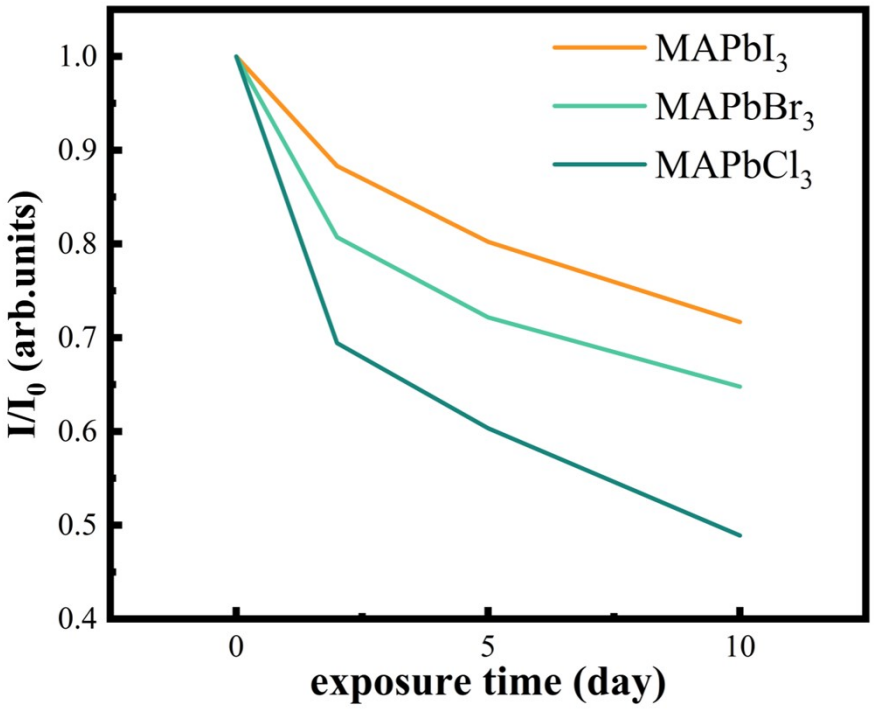

Figure S16. The luminescence intensity of $MAPbI_3$, $MAPbBr_3$, and $MAPbCl_3$ decreases over time.

Reference:

1. Ma, J.; Zhao, Z.; Yi, X.; Chen, J.; Hong, L.; Chi, E. H.; Acm In Modeling Task Relationships in Multi-task Learning with Multi-gate Mixture-of-Experts, 24th ACM SIGKDD Conference on Knowledge Discovery and Data Mining (KDD), London, ENGLAND, 2018Aug 19-23; London, ENGLAND, 2018; pp 1930-1939.

2. Hou, Q.; Zhou, D.; Feng, J.; Ieee Comp, S. O. C. In Coordinate Attention for Efficient Mobile Network Design, IEEE/CVF Conference on Computer Vision and Pattern Recognition (CVPR), Electr Network, 2021Jun 19-25; Electr Network, 2021; pp 13708-13717.

3. Ancona, M.; Ceolini, E.; Öztireli, C.; Gross, M., Towards better understanding of gradient-based attribution methods for Deep Neural Networks. Arxiv 2018.

4. Matheu, R.; Vigil, J. A.; Crace, E. J.; Karunadasa, H. I., The halogen chemistry of halide perovskites. Trends in Chemistry 2022, 4 (3), 206-219.

5. Akman, E.; Ozturk, T.; Xiang, W.; Sadegh, F.; Prochowicz, D.; Tavakoli, M. M.; Yadav, P.; Yilmaz, M.; Akin, S., The effect of B-site doping in all-inorganic CsPbIBr3 absorbers on the performance and stability of perovskite photovoltaics. Energy & Environmental Science 2023, 16 (2), 372-403.

6. Lu, C.-H.; Biesold-McGee, G. V.; Liu, Y.; Kang, Z.; Lin, Z., Doping and ion substitution in colloidal metal halide perovskite nanocrystals. Chemical Society Reviews 2020, 49 (14), 4953-5007.